Science of the Total Environment 557–558 (2016) 520–530

Contents lists available at ScienceDirect

Science of the Total Environment

journal homepage: www.elsevier.com/locate/scitotenv

Characteristics of carbonaceous aerosols: Impact of biomass burning and secondary formation in summertime in a rural area of the North China Plain

Lan Yao [a], Lingxiao Yang [a,b,*], Jianmin Chen [a,b,c], Xinfeng Wang [a], Likun Xue [a], Weijun Li [a], Xiao Sui [a], Liang Wen [a], Jianwei Chi [a], Yanhong Zhu [a], Junmei Zhang [a], Caihong Xu [a], Tong Zhu [d], Wenxing Wang [a]

[a] Environment Research Institute, Shandong University, Jinan 250100, China
[b] School of Environmental Science and Engineering, Shandong University, Jinan 250100, China
[c] Key Laboratory of Atmospheric Particle Pollution and Prevention (LAP3), Fudan Tyndall Centre, Department of Environmental Science and Engineering, Fudan University, Shanghai 200433, China
[d] State Key Laboratory for Environment Simulation and Pollution Control, College of Environmental Sciences and Engineering, Peking University, Beijing 100871, China

HIGHLIGHTS

- OM/OC ratio (2.07) was calculated to estimate organics at rural areas in NCP.
- Biomass burning contribution to carbonaceous aerosols was quantified.
- SOA formation was investigated based on VOCs evolution.

GRAPHICAL ABSTRACT

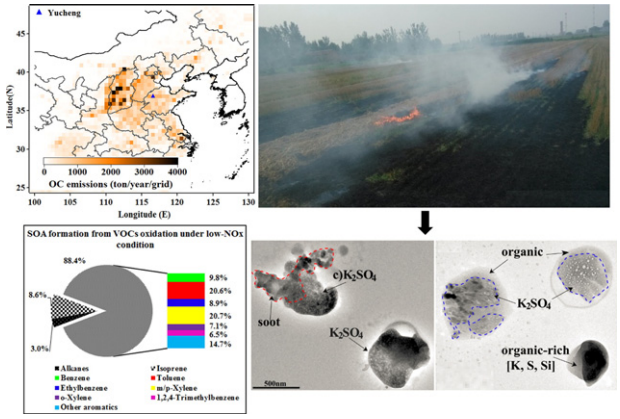

ARTICLE INFO

Article history:
Received 14 December 2015
Received in revised form 20 February 2016
Accepted 16 March 2016
Available online 29 March 2016

Editor: D. Barcelo

Keywords:
Carbonaceous aerosols
OM/OC ratio
Biomass burning
SOA formation

ABSTRACT

To determine the characteristics of carbonaceous aerosols in rural areas of the North China Plain, field measurements were conducted at Yucheng (YC) in the summers of 2013 and 2014. The concentrations of carbonaceous aerosols at YC exhibited clear diurnal variation, with higher concentrations in the early morning and at night and lower concentrations during the afternoon hours. The mass-balance method designed for particulate matter smaller than 2.5 μm ($PM_{2.5}$) was used to calculate the organic matter (OM)/organic carbon (OC) ratio. The value obtained, 2.07 ± 0.05, was suggested as a reference to estimate organics in $PM_{2.5}$ in rural areas of the North China Plain. Biomass burning was identified to be a significant source of carbonaceous aerosols; approximately half of the samples obtained at YC were affected by biomass burning during summer 2013. Case studies revealed that biomass burning accounted for up to 52.6% of the OC and 51.1% of the elemental carbon in $PM_{2.5}$ samples. The organic coatings observed on sulphur-rich and potassium-rich particles indicated the formation of secondary organic aerosols (SOA) from the oxidation of precursor volatile organic compounds (VOCs) during the aging of smoke released from biomass burning. Based on the evolution of the VOCs, the contribution of VOCs

* Corresponding author.
E-mail address: yanglingxiao@sdu.edu.cn (L. Yang).

http://dx.doi.org/10.1016/j.scitotenv.2016.03.111

oxidation to SOA concentration was 3.21 and 1.07 μg m^{-3} ppm^{-1} CO under conditions of low nitrogen oxide (NOx) and high NOx, respectively. Aromatics (e.g. benzene, toluene, xylene and ethylbenzene) made the greatest contribution to SOA concentration (88.4% in low-NOx conditions and 80.6% in high-NOx conditions). The results of the study offer novel insights into the effects of biomass burning on the carbonaceous aerosols and SOA formation in polluted rural areas.

1. Introduction

Carbonaceous aerosols, composed mainly of organic carbon (OC) and elemental carbon (EC), play important roles in human health, radiative forcing and climate change, as they make up a significant proportion of particulate matter smaller than 2.5 μm ($PM_{2.5}$) (Jacobson, 2001; Mauderly and Chow, 2008). OC, a complex mixture of hundreds of organic compounds (e.g. polycyclic aromatic hydrocarbons, PAHs), is associated with respiratory and cardiovascular disease, and may even cause cancer (Mauderly and Chow, 2008). EC is a major absorber of visible solar radiation in the atmosphere, and has been identified as the second greatest contributor to global warming in the troposphere, after carbon dioxide (CO_2) (Ramanathan and Carmichael, 2008). Of the numerous anthropogenic sources of carbonaceous-aerosol emissions, such as power plants, industrial production, residential and transportation, biomass burning has been reported to be the largest global source of OC and EC (Cheng et al., 2013). OC is either emitted directly from combustion sources, which is primary OC (POC), or formed as secondary OC (SOC) from the photochemical reactions of precursor volatile organic compounds (VOCs) with either hydroxyl (OH) radicals and ozone (O_3) (predominantly during the daytime) or nitrate (NO_3) radicals (during the night) (Lambe et al., 2015; Rollins et al., 2012).

North China Plain (NCP) suffered from serious air pollution. Zhang et al modeled the emission of carbonaceous aerosols over China (Zhang et al., 2009) and proposed far more OC is emitted in the NCP region than in other areas of China (Fig. 1). Thus, intensive studies on carbonaceous compounds, including seasonal variation, spatial distribution, sources and biomass burning impact, have been conducted in the NCP region (Cheng et al., 2013; Fu et al., 2012b; Li and Bai, 2009; Pathak et al., 2011; Yang et al., 2011; Zhao et al., 2013). Biomass burning has an influence on carbonaceous aerosols level in NCP (Cheng et al., 2013; Fu et al., 2012b), however, quantitative data on the contribution

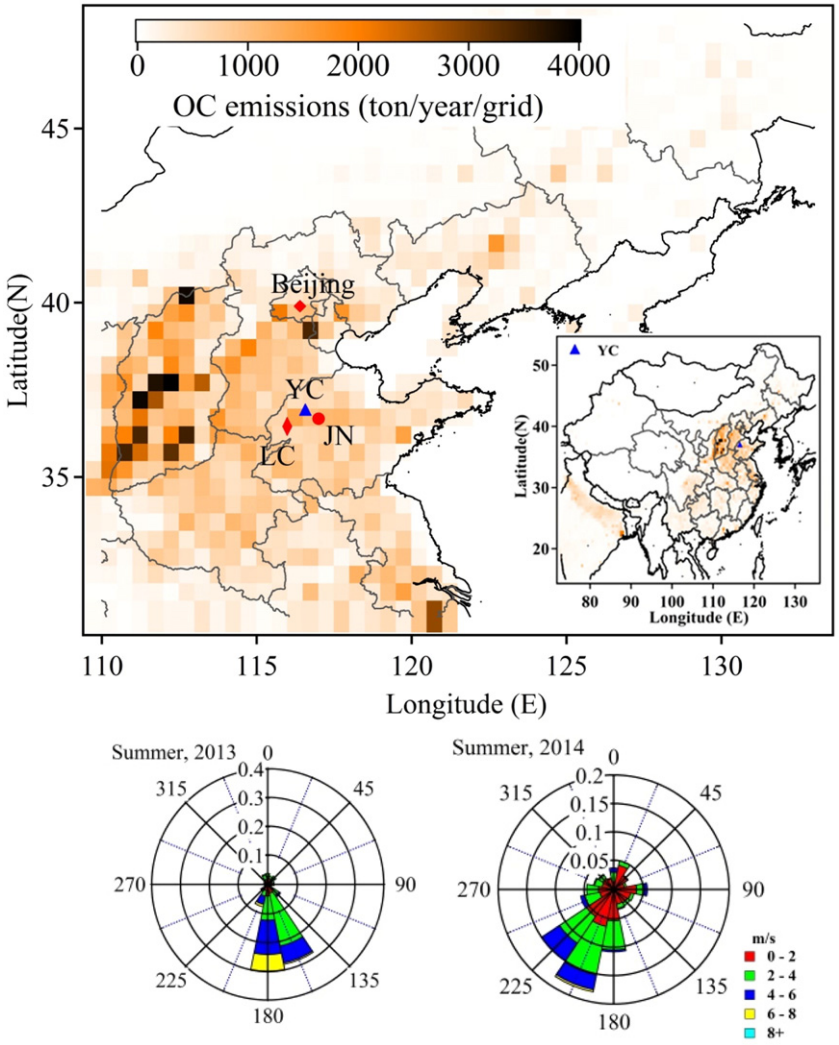

Fig. 1. OC emissions over China (Zhang et al., 2009). The blue marker is the sampling site, YC. LC: Liaocheng; JN: Jinan; Winds at YC during summer in 2013 and 2014 are also shown.

of biomass burning to carbonaceous aerosols in the NCP region was limited in Beijing (Cheng et al., 2013; Duan et al., 2004; Zhang et al., 2008b). Little quantitative data on carbonaceous aerosols emitted from biomass burning was reported in rural areas in NCP. Organic matter (OM) accounts for a significant proportion of $PM_{2.5}$ (20–50%), which may reach 80% in special environment (rainforest, Chen et al., 2015). OM/OC ratio, widely used to estimate OM because OM has seldom been measured directly due to the expensive instruments (e.g. aerosol mass spectrometers), has been reported between 1.2 and 2.6, depending on different seasons and sources (Aiken et al., 2008; Bae et al., 2006; Russell, 2003; Turpin and Lim, 2001). However, investigation on OM/OC ratio was limited in urban areas in northern China (Xing et al., 2013). Little information on the OM/OC ratio in rural areas of northern China has been obtained.

Given the limitations of previous research, we decided to investigate the impact of biomass burning on carbonaceous components and SOA formation from VOC oxidation in a rural site. Yucheng (YC), a rural receptor site at the centre of the NCP (Fig. 1), was selected as a sampling site. High time resolved (1 h) carbonaceous aerosols were characterised during the summers of 2013 and 2014. An OC to OM conversion factor was calculated to provide a reference for estimating organics in rural areas of northern China. The contribution of biomass burning to carbonaceous aerosol was quantified, and the mixing states of individual particles during typical biomass burning events were analysed. In addition, the process of SOA formation from VOC oxidation was investigated. The study's findings provide new data to support future studies and offer guidelines for regional air quality improvement strategies.

2. Experiment

2.1. Sampling and instruments

The measurements were obtained at the Chinese Academy of Sciences Comprehensive Station in YC (36°52′N, 116°34′E), Shandong Province (Fig. 1) from 2 June to 6 July 2013 and from 5 June to 15 July 2014. YC, with a population of 520,000, is located 50 km northwest of Jinan (the capital of Shandong Province, with a population of 7 million) and 67 km northeast of Liaocheng (with a population of 6 million). When the wind blows from the south or southwest, YC is downwind of Jinan and Liaocheng (Fig. 1). The sampling site is surrounded by farmland, with few nearby emission sources. A highway (G308) is situated 1.5 km south of the site.

The instruments were installed on a mobile monitoring platform (6.8 m × 2.7 m × 2.4 m) next to open cropland. The inlets of the samplers were fixed at ~1.5 m above the roof of the container. Hourly OC and EC measurements were taken using a semi-continuous thermal-optical carbon analyser (Sunset Laboratory, Inc.) with a flow rate of 8 L min^{-1}. $PM_{2.5}$ was measured using a real-time PM monitor (operating at 16.67 L min^{-1}) capable of providing 1-min measurements (SHARP 5030, Thermo). The PM monitor measured ambient aerosol concentration based on aerosol light scattering (nephelometry) and beta attenuation. The average $PM_{2.5}$ concentration is calculated from individual cyclic concentration measurements. All valid cyclic concentration values are summed either as a 30-min or 60-min average concentration being calculated. If at least 2/3rds of the cyclic concentration measurements are valid, the average is considered to be valid. Before and after the campaign, the necessary sensor calibrations, including temperature, relative humidity, barometric pressure and flow rate were conducted. Mass calibration was performed using a series of null and standard foils (Thermo Fisher Scientific). Water-soluble ions such as sulphate (SO_4^{2-}), nitrate (NO_3^-), chloride (Cl^-), sodium (Na^+), ammonium (NH_4^+), potassium (K^+), magnesium (Mg^{2+}) and calcium (Ca^{2+}) ions were analysed by online ion chromatography (MARGA, Applikon,) with a 1-h time resolution, at flow rate of 16.7 L min^{-1} (Wen et al. 2015). A solution of lithium bromide (LiBr, 4.0 mg L^{-1}) was periodically injected as an internal standard. Multi-point calibrations of the target water-soluble ions were performed before and after the campaign. Trace gases, including O_3, carbon monoxide (CO) and nitrogen oxide (NOx; NO + NO_2), were detected in real time (Xue et al., 2011). Data on the meteorological parameters (e.g. temperature, relative humidity, wind and precipitation) were provided by the Chinese Academy of Sciences Comprehensive Station.

Air samples were collected in 3.2-L canisters (Entech Instruments, Inc., Simi Valley, CA, US) for VOC analysis. Before sampling, the canisters were evacuated to <100 mtorr and then pressurised to 20 psi with high-purity nitrogen. After 3 cycles of evacuation and refilling, the canisters were evacuated to <20 mtorr for use. Most of the samples were collected at 13:00 each day from 5 June to 8 July 2014. On 12 June, 18 June and 8 July 2014, samples were taken every 2 h between 7:00 and 19:00 and from 23:00 onward to examine their diurnal variation. Fifty canister samples were obtained.

2.2. Method

OC and EC were analysed using the thermal-optical transmittance method. First, the sampled air was passed through a parallel-plate organic denuder (Sunset Laboratory, Inc.) to remove gaseous organic matter, and the particles were collected on a mounted quartz filter. Next, stepwise heating programmes were performed (300–500–650 °C in a helium (He) atmosphere and 550–700–870 °C in an oxidising atmosphere (95% He + 5% O_2). After passing through a manganese dioxide oxidising oven, the carbonaceous species were converted to CO_2 and then detected by a nondispersive infrared detector. The OC/EC split point depends on changes in laser (660 nm, passing through the mounted filter) intensity during the analysis. A known volume of methane (CH_4) at a known concentration (5% CH_4 + 95% He) was injected as an internal standard during each cycle of analysis. Before and after the campaign, calibration was performed using a series of sucrose standard solutions (slope = 1.04, r^2 = 0.999). A new filter was mounted every 3 days to maintain laser transmittance, as minerals resistant to carbonising would residue on the filter, affecting laser transmittance. The detection limits for OC and EC were both 0.3 μgC m^{-3} (based on the flow rate of 8 L min^{-1} and a 43 min sampling time), and the principles were as described by Wang et al. (2011).

Based on US EPA Method TO-15, C2-C11 non-methane hydrocarbons (NMHCs) including 29 alkanes, 11 alkenes and 16 aromatics, were detected using a system consisting of a cryogenic preconcentrator (Model 7100, Entech Instruments, Inc., Simi Valley, CA, US), a gas chromatograph (HP-7890A, Hewlett Packard Co., Palo Alto, CA, US) equipped with a quadrupole mass spectrometer (HP-5975C, Hewlett Packard), and a flame-ionisation detector. Detailed descriptions of the analytical method and calibration process can be found in Wang et al. (2010) and our most recent study (Zhu et al., 2015).

To investigate the mixing states of the carbonaceous particles, single-particle samples were collected during two typical biomass burning events (13 June and 16 June 2013). An impactor with a 0.5 mm diameter jet nozzle was used to collect the particles on transmission electron microscopy (TEM) copper grids coated with carbon (carbon type-B, 300-mesh copper, Tianld Co., China) at a flow rate of 1.0 L min^{-1}. The sampling time was 30–120 s, depending on $PM_{2.5}$ concentration. A combination of TEM and energy-dispersive X-ray (EDX) spectroscopy was used to obtain information on the morphology, mixing state and composition of individual particles. Detailed information on TEM analysis can be found elsewhere (Li and Shao, 2010; Li et al., 2010).

The EC-tracer method has been widely used to estimate SOC concentration (Cao et al., 2007; Wang et al., 2012; Zhou et al., 2012). Although this simple method may be of certain uncertainty, the integration of high time resolved data yields detailed information on SOC formation,

such as diurnal variation in SOC. SOC was estimated from the following equations:

$$SOC = OC - POC \quad (1)$$

$$POC = (OC/EC)_{pri} + OC_{noncombustion} \quad (2)$$

where $(OC/EC)_{pri}$ and $OC_{noncombustion}$ denote the minimum OC/EC ratio and OC not produced from combustion, respectively. The key parameter used to calculate SOC was $(OC/EC)_{pri}$. $(OC/EC)_{pri}$ is usually determined by least-squares regression, using samples with OC/EC ratios in the lowest 5–20% (Cao et al., 2007) which depends on the number of samples. Based on our data set, we excluded data significantly influenced by rain, and selected OC/EC ratios in the lowest 10%. $(OC/EC)_{pri}$ was 2.24 ($r^2 = 0.87$) and 2.01 ($r^2 = 0.93$) at YC in summer 2013 and summer 2014, respectively.

The Hybrid Single-Particle Lagrangian Integrated Trajectory (HYSPLIT, Version 4.9) model was used to calculate air mass back trajectories. The meteorological data used was downloaded from the web site of ftp://arlftp.arlhq.noaa.gov/pub/archives/gdas1/. As the online data obtained were of 1-h time resolution, HYPLIT was run every hour at a starting height of 50 m AGL. For vertical motion, we select the default option, which uses the meteorological model's vertical velocity fields.

3. Results and discussion

3.1. Overview of data

Fig. 2 depicts the time-series variation obtained for OC, EC, $PM_{2.5}$, trace gases and meteorological factors (1 h time resolution) during the summers of 2013 and 2014. Table 1 provides statistical information on carbonaceous components, $PM_{2.5}$ and meteorological parameters at YC in summer 2013 and summer 2014. The concentrations of OC, EC and $PM_{2.5}$ at YC in summer 2013 were 10.80 ± 6.95 μgC m^{-3}, 2.42 ± 1.35 μgC m^{-3} and 132.3 ± 89.2 μg m^{-3}, respectively; those in summer 2014 were 8.05 ± 4.48 μgC m^{-3}, 1.51 ± 1.02 μgC m^{-3} and 99.2 ± 54.5 μg m^{-3}, respectively. An independent-samples *t*-test was performed using version 21 of the Statistical Package for the Social Sciences software to test the significance of the differences between pollutant concentrations in 2013 and 2014. The OC, EC and $PM_{2.5}$ concentrations measured in 2013 were significantly ($p < 0.001$) higher than those obtained in 2014. The number of fire detections was 52.5% more in the region in 2013 than in 2014 (fire data obtained from http://hjj.mep.gov.cn/stjc/201407/P020140710408678423165.pdf), consistent with the finding that concentrations of K^+ (a traditional biomass burning indicator) at YC in 2013 were much higher than those in 2014 (Table 1). The concentrations of carbonaceous species in YC were higher than that in

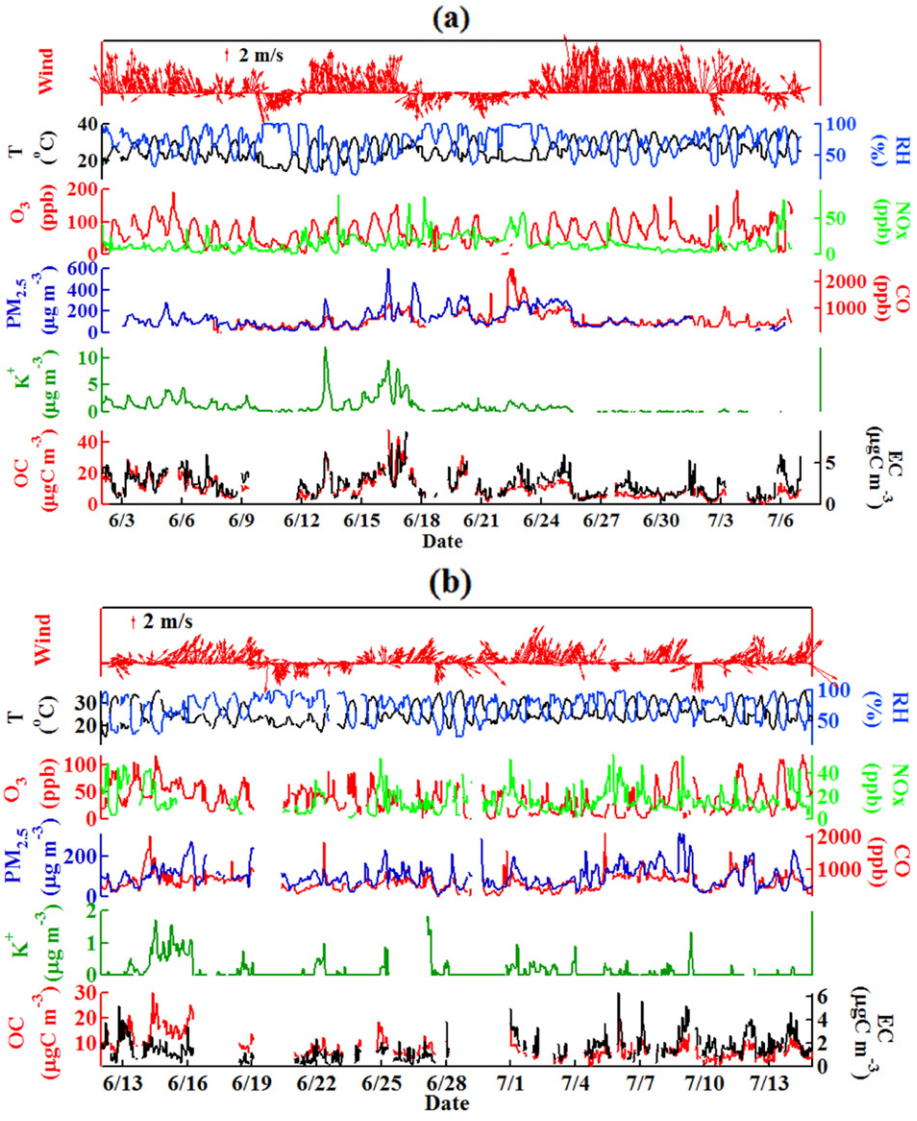

Fig. 2. Time series of carbonaceous species, $PM_{2.5}$, trace gases and meteorological parameters (1 h time resolution) during summer of (a) 2013 and (b) 2014.

Table 1
Statistics of OC, EC and meteorological parameters at YC in summer of 2013 and 2014.

	6/2–7/6, 2013			6/12–7/15, 2014		
	Average	Min	Max	Average	Min	Max
OC (μgC m^{-3})	10.80 ± 6.95	0.31	48.09	8.05 ± 4.48	0.53	29.95
EC (μgC m^{-3})	2.42 ± 1.35	BDL	7.35	1.51 ± 1.02	BDL	6.32
SOC/OC (%)	45.8 ± 18.1	–	82.4	54.8 ± 21.7	–	85.1
$PM_{2.5}$ (μg m^{-3})	132.3 ± 89.2	14.7	599.8	99.2 ± 54.5	9.4	314.4
TC/$PM_{2.5}$ (%)	11.8 ± 5.8	4.3	32.8	10.9 ± 5.7	4.1	35.4
K^+ (μg m^{-3})	1.17 ± 1.57	BDL	12.03	0.13 ± 0.28	BDL	1.83
T (°C)	25.9 ± 5.1	13.7	38.6	25.7 ± 4.5	15.0	35.9
RH (%)	70.6 ± 21.1	17.0	100.0	71.8 ± 18.8	23.0	100.0
WS (m s^{-1})	2.8 ± 1.8	0	9.5	1.9 ± 1.5	0	6.6
WD	South/ southeast	–	–	Southwest	–	–

±: standard deviation; BDL: below detection limit.

a rural background site in Europe (4.0 ± 2.4 μgC m^{-3} for OC and 0.9 ± 0.5 μgC m^{-3} for EC, Gilardoni et al., 2011), a rural site in southeastern United States (2.81 μgC m^{-3} for OC and 0.56 μgC m^{-3} for EC, Liu et al., 2005) and a rural northeastern US area (1.79 μgC m^{-3} for OC and 0.31 μgC m^{-3} for EC, Kim and Hopke, 2004).

SOC accounted for 45.8 ± 18.1% and 54.6 ± 21.7% of the OC measured during summer 2013 and summer 2014, respectively, with an average SOC/OC ratio of 50.2 ± 20.7%. The proportion of SOC was comparable with that measured at a rural site in Jinan (47.5%, Yang et al., 2012), but lower than that measured at Mount Tai (73.4%, Wang et al., 2012), a remote high-altitude area of the NCP. Similar proportions of total carbon (TC; TC = OC + EC) in $PM_{2.5}$ were obtained in the two summers (11.8 ± 5.8% in 2013 and 10.9 ± 5.7% in 2014). These values were comparable with observations made at Shangdianzi (12.9%), a regional background site near Beijing (Zhao et al., 2013). Meteorological factors (e.g. wind) usually have a significant influence on pollutant levels. Wind plays a role in diluting pollutants in the atmosphere and transporting pollutants from more polluted urban areas to rural areas. In 2013, the wind at YC came from the south and southeast; in 2014, YC was controlled by southwesterly wind with a lower speed (Fig. 1). As the concentrations of OC and EC displayed similar relationship with wind speed, here only EC–wind speed relationship was shown during the two summers (Fig. 3). Generally, the trends of EC concentrations were decreasing with increasing wind speed during the two summer periods. In the summer of 2014, EC concentration decreased significantly with increasing wind speed in the lower wind speed range and remained stable at lower concentration in the higher wind speed range (Fig. 3), which was similar with that in urban areas (Tokyo, Kondo et al., 2006). However, the concentration of EC did not show obvious variation when wind speed was less than around 4 m s^{-1} in the summer of 2013 (Fig. 3), which was probably caused by the transportation of frequent biomass burning. For example, with higher wind speed blowing from the south, the concentrations of OC and EC peaked on 13 June 2013 (Fig. 2), which was likely resulted from long range transport of biomass burning (discussed in Section 3.3).

Fig. 4 shows the diurnal variation in OC, EC, related pollutants and meteorological parameters during the summer sampling period in 2013 and 2014, respectively. Similar diurnal variations in the carbonaceous components were observed in the two summers. The concentrations of OC and EC exhibited consistent diurnal patterns, with peaks at around 0700 LT and 2000 LT. OC and EC were observed to be at lowest concentrations in the afternoon hours. Compared with EC, the concentration of OC decreased at a slower rate, which was probably due to SOC formation during the day. The diurnal pattern of OC and EC was associated with meteorological conditions. The lower concentrations in the afternoon hours were attributed to the dilution of aerosols related to the elevated planetary boundary layer (PBL) and higher wind speed. The formation of a nocturnal boundary layer and stagnant air favor the accumulation of pollutants, causing increased concentrations of pollutants at night and early morning hours (Sahu et al., 2011). Temperature has a significant effect on the gas/particle partitioning of semivolatile organic compounds (SVOCs) in the atmosphere (Cousins et al., 1999). Cooler nighttime temperature may favor gas/particle-phase equilibrium to move towards the particle phase, leading to the adsorption and condensation of SVOCs onto particles (Lamorena and Lee, 2008). The SOC/OC ratio clearly increased during the day and presented good correlation with O_3, indicating SOC formation from photochemical processes during the day.

3.2. OM/OC ratio ($f_{OM/OC}$)

To provide a reference for the estimation of organics in rural areas of northern China, the OM/OC ratio ($f_{OM/OC}$) was calculated using the $PM_{2.5}$ mass balance method, which was successfully used to calculate $f_{OM/OC}$ by Bressi et al. (2013). Xing et al. (2013) pointed out that the mass-balance method may lead researchers to over-estimate the OM/OC ratio, mainly due to significant nitrate loss during summer (50–70%) based on filter sampling. As we used online measurements of $PM_{2.5}$ and its composition, the uncertainty of the method was greatly reduced. The following is a simple description of the method:

$$[OM] = f_{OM/OC} \times [OC] \quad (3)$$

$$f_{OM/OC} = \frac{([PM_{2.5}] - [\text{Sea Salt}] - [\text{Dust}] - [\text{Main Inorganic Ions}] - [EC])}{[OC]} \quad (4)$$

$$[\text{Sea Salt}] = [Na^+] + [\text{ss-}Cl^-] + \left[\text{ss-}SO_4^{2-}\right] + \left[\text{ss-}Mg^{2+}\right] + \left[\text{ss-}Ca^{2+}\right] + [\text{ss-}K^+] = 3.24 \times [Na^+] \quad (5)$$

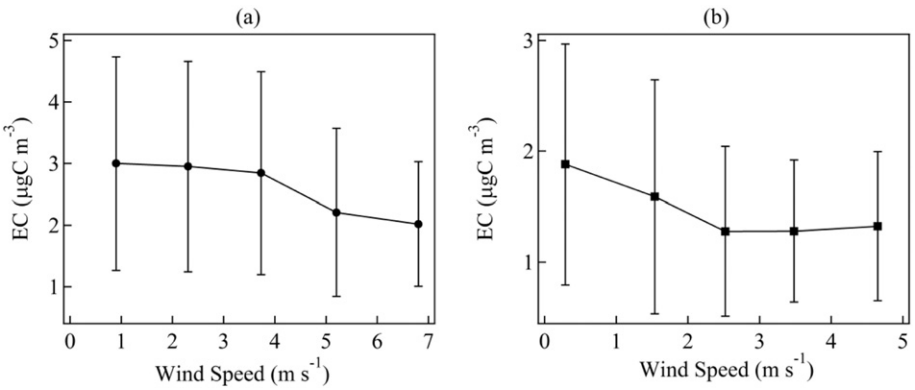

Fig. 3. The relationship between EC concentrations and wind speed during summer in (a) 2013 and (b) 2014. Bars represent standard deviation.

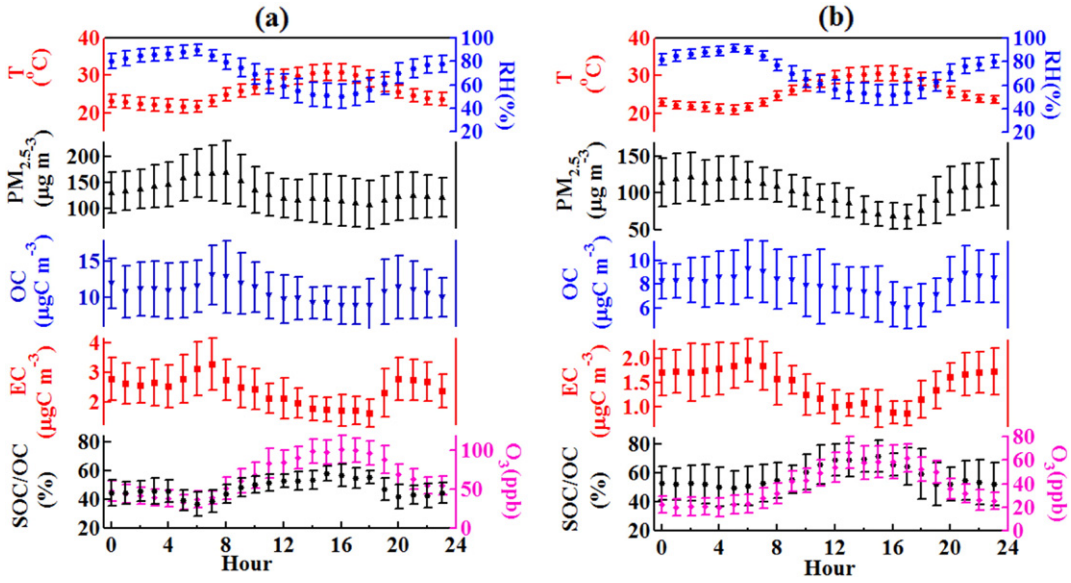

Fig. 4. Diurnal variations of carbonaceous species and meteorological factors at YC in the summer sampling period in (a) 2013 and (b) 2014, respectively. Error bars indicate half of standard deviation.

$$[\text{Dust}] = \left[\text{nss-Ca}^{2+}\right]/0.11 \quad (6)$$

$$[\text{Main Inorganic Ions}] = \left[\text{na}-\text{SO}_4^{2-}\right] + \left[\text{NO}_3^-\right] + \left[\text{NH}_4^+\right] + [\text{nss}-\text{Cl}^-] + [\text{nss}-\text{K}^+] \quad (7)$$

where 'ss-' and 'nss-' indicate sea salt and non-sea salt, respectively. Based on seawater ion ratios (Seinfeld and Pandis, 1998), $[\text{ss-Ca}^{2+}] = 0.038[\text{Na}^+]$, $[\text{ss-SO}_4^{2-}] = 0.251[\text{Na}^+]$, $[\text{ss-Cl}^-] = 1.798[\text{Na}^+]$ and $[\text{ss-K}^+] = 0.036[\text{Na}^+]$.

We made minor changes to the method proposed by Bressi et al. (2013) to suit our samples. In the previous study, [Sea Salt] = $[\text{Na}^+] + [\text{Cl}^-] + [\text{ss-Mg}^{2+}] + [\text{ss-K}^+] + [\text{ss-Ca}^{2+}] + [\text{ss-SO}_4^{2-}]$. However, not all Cl^- originates from sea salt. In the current study, biomass burning was found to be a significant source of Cl^-. Therefore, we estimated sea salt by multiplying $[\text{Na}^+]$ by 3.24, based on the relationships previously identified between Na^+ and other ions in sea water (Seinfeld and Pandis, 1998). Unlike Bressi et al. (2013), we considered nss-Cl^- and nss-K^+ when identifying the main inorganic ions, due to the influence of biomass burning. As calcium is a typical element of dust, Ca^{2+} is often used to estimate atmospheric dust concentration (Guinot et al., 2007). We used the average nss-Ca^{2+}/dust conversion factor (0.11) obtained for Beijing in the summer (Guinot et al., 2007) to estimate dust concentration. Values of $f_{OM/OC}$ smaller than 1 and >3 were excluded (physically meaningless). Effective data made up approximately 70% of the observations (effective data numbers were 452 and 250 for 2013 and 2014, respectively).

We explored the relationship between OC and OM using linear least squares fitting, with the intercept forced to zero. The data obtained for $f_{OM/OC}$ at YC are depicted in Fig. 5. OC concentration was highly correlated with OM concentration ($r^2 = 0.95$ and 0.93 for the summers of 2013 and 2014, respectively). $f_{OM/OC}$ values of 2.09 ± 0.05 and 2.05 ± 0.08 were obtained in YC in summer 2013 and summer 2014, respectively, with an average of 2.07 ± 0.05. These results were consistent with observations made in nonurban areas (2.1 ± 0.2) by Turpin and Lim (2001). Comparable results (2.03–2.12) have also been obtained at rural sites in France (Bressi et al., 2013). However, different values of $f_{OM/OC}$ were reported at a suburban site in the Yangtze River Delta (1.55, Huang et al., 2013) and a rural site downwind of the highly polluted central area of the Pearl River Delta (1.77 ± 0.08, Huang et al., 2011), indicating that the characteristics of organic aerosols in the NCP region differ from those in southern China. Guinot et al. (2007) reported $f_{OM/OC}$ values of 1.55–1.75 in Beijing and 1.4 in Paris. The $f_{OM/OC}$ values obtained in the current study were higher than those in urban areas because aerosols tend to become more oxygenated as they age, increasing their average organic molecular weight per carbon weight (Turpin and Lim, 2001). Therefore, 2.07 was identified as a suitable OM/OC ratio for nonurban areas of the NCP.

3.3. Biomass burning

3.3.1. Identification of biomass burning

Biomass burning is generally characterised by a high potassium content, and the mass ratio of excess potassium (the proportion not attributed to soil dust or sea salt) to EC (K^+_{excess}/EC) indicates the relative contributions of biomass burning and fossil-fuel combustion to carbonaceous-aerosol concentration (Cachier et al., 1995; Chen et al.,

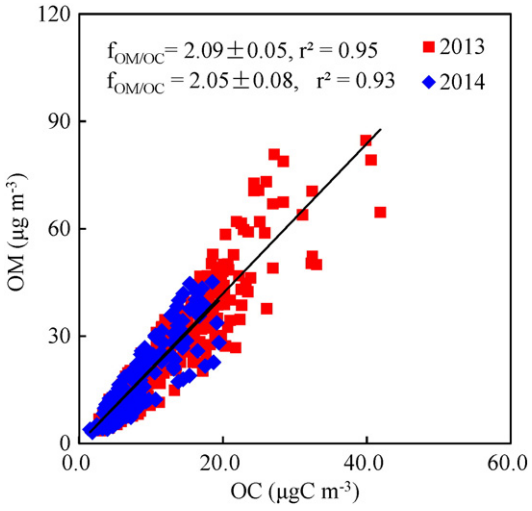

Fig. 5. Relationship between OC and OM during summer of 2013 and 2014 at YC. Uncertainties are 95% confidence intervals.

2014). K^+_{excess} is defined as follows:

$$K^+_{excess} = K^+_{total} - K^+_{soil} - K^+_{sea\ salt} \quad (8)$$

$$K^+_{soil} = 0.91Ca^{2+} \quad (9)$$

$$K^+_{sea\ salt} = 0.36Na^+ \quad (10)$$

K^+_{soil} was estimated from the K/Ca ratio (0.91) in the soil (Yan et al., 1997), and $K^+_{sea\ salt}$ was estimated by multiplying Na^+ by 0.036, based on the K/Na ratio in sea water (Seinfeld and Pandis, 1998). The K^+_{excess}/EC ratio for YC ranged from 0 to 2.13, with an average of 0.18 ± 0.31. Similar results were obtained in three cities in China's Sichuan Basin (average = 0.12–0.20), all of which were affected by biomass burning (Chen et al., 2014). Assuming K^+_{excess} was emitted from biomass burning, we considered YC to be affected by biomass burning when K^+_{excess} was >0. The statistical results indicated that the samples taken at YC in summer 2013 were significantly affected by biomass burning on approximately 16 of the 34 sampling days (Fig. 6). We selected two typical biomass burning events (BB1 and BB2, Fig. 6), for the following reasons. (1) During both events, the K^+ level dramatically increased, reaching a maximum hourly concentration of 12.03 μg m^{-3} on 13 June (BB1) and 9.62 μg m^{-3} on 16 June (BB2). These values were 8 and 10 times higher, respectively, than the average. The observed K^+ peaks were accompanied by high concentrations of OC and EC. (2) A 48-h air mass back trajectory and hotspots map (data source: the website of Ministry of Environment Protection of People's Republic of China, http://hjj.mep.gov.cn/stjc/index_13.htm, Fig. 7) revealed intensive hotspots south of YC, and the air mass at YC during BB1 and BB2 originated from the south, passing through biomass burning areas.

Fig. 8 shows the particle composition of samples collected during BB1 (left, 13 June, 08:00) and BB2 (right, 16 June, 08:00). Soot particles are easily recognisable, due to their unique morphology. Fresh soot aggregates are typically small, spherical elementary carbonaceous particles that cluster together to form straight or branched chains. In our samples, soot particles were aggregated with larger K-rich and sulphur (S)-rich particles (Fig. 8c), modifying the morphology of the soot (Fig. 8a). This indicated that the smoke emitted from biomass burning had undergone atmospheric aging during long-range transport. Once emitted into the atmosphere, soot can be oxidised by O_3, OH, SO_2 and NO_2, leading to a collapsed graphitic structure (Khalizov et al., 2013; Zhang et al., 2008a). K-rich and S-rich particles with an organic coating (Fig. 8b) were identified in the sample. The coating of K- and S-rich particles has been shown to be water-soluble (Li and Shao, 2010), determining the particles' hygroscopicity, ability to act as cloud condensation nuclei and heterogeneous chemical reactivity. Their organic coating is believed to comprise SOA formed in the atmosphere when the products of VOC oxidation condense on inorganic particles (Li et al., 2010). The high ozone levels (65 ± 35 ppb) observed at YC suggest that the formation and subsequent condensation of SOA may be an important pathway of this organic coating formation (Fu et al., 2012a). Spherical organic-rich particles similar to tar balls were observed in the TEM images (Fig. 8d). EDX spectra revealed that these particles consisted of abundant C, with trace amounts of S, K and silicon, indicating that they originated from young biomass burning smoke.

3.3.2. Biomass burning contribution

We estimated the contribution of biomass burning using the K^+-tracer method, as K^+ is an indicator of biomass burning. The method has been used by Chen et al. (2014), and can be represented as follows:

$$OC = POC + SOC \quad (11)$$

$$POC = POC_{ff} + POC_{bb} \quad (12)$$

$$OC_{ff} = (OC/EC)_{ff} \times EC_{ff} \quad (13)$$

$$OC_{bb} = (OC/EC)_{bb} \times EC_{bb} \quad (14)$$

$$EC = EC_{ff} + EC_{bb} \quad (15)$$

$$EC_{bb} = \frac{1}{(K^+/EC)_{bb}} \times K^+_{bb}. \quad (16)$$

The subscripts ff and bb denote fossil-fuel combustion and biomass burning, respectively. $(OC/EC)_{bb}$ and $(K^+/EC)_{bb}$ in Eq. (14) and Eq. (16) represent the source emissions of biomass burning in the study area. We used the local biomass burning source profile obtained by Li et al. (2007). The open burning of biomass (wheat straw and maize stover) and field measurements were carried out at a rural site in Shandong Province. As wheat is harvested in this region in mid-June, we selected $(OC/EC)_{bb}$ and $(K^+/EC)_{bb}$ values of 5.03 and 1.30, respectively, for wheat-straw burning. $(OC/EC)_{ff}$ can be represented by $(OC/EC)_{pri}$, which was calculated using the EC-tracer method described in Section 2.2. As biomass burning occurred frequently during the summer of 2013, the $(OC/EC)_{ff}$ value obtained

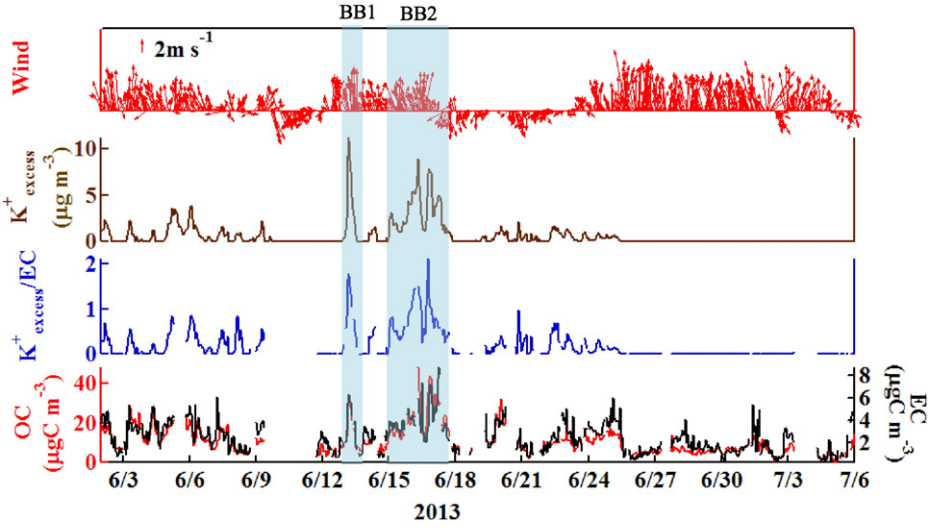

Fig. 6. Overview of biomass burning influence on carbonaceous species at YC during the summer, 2013.

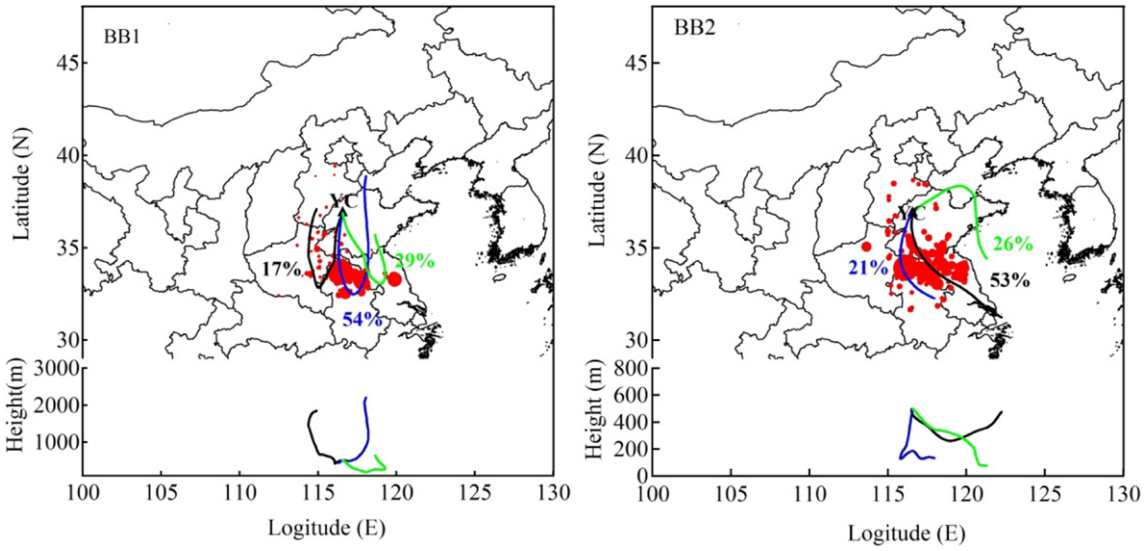

Fig. 7. 48-h air mass back trajectory and hotspots map in BB1 and BB2, respectively. Hotspots data were downloaded from the website of Ministry of Environment Protection of the People's Republic of China (http://hjj.mep.gov.cn/stjc/index_13.htm).

in summer 2014 (2.01) was selected. We used K^+_{excess}, as defined in Section 3.1, to evaluate K^+_{bb}.

Table 2 shows the contribution of biomass burning to the presence of carbonaceous aerosols during typical biomass burning events (BB1 and BB2) and throughout the summer of 2013. Approximately half of the carbonaceous components during BB1 and BB2 (52.6% OC and 51.1% EC in BB1; 44.5% OC and 50.8% BB2) were attributed to biomass burning. The contribution of biomass burning to the OC measured at YC was similar to that reported in Daejeon, Korea during harvesting (45%) (Jung et al., 2014). However, the contribution of biomass burning to EC at YC was greater than that in Daejeon (12%, Jung et al., 2014), indicating that biomass burning was a more important source of EC at YC. Biomass burning contribution to the carbonaceous aerosols measured at YC was much higher than that at the urban background site Zurich in summer (6% ± 2 for EC and 10 ± 2% for OC, Szidat et al., 2006). Fossil-fuel combustion contributed a lower fraction to the OC measured during BB1 (20.0%) and BB2 (17.2%).

3.4. Contribution of VOC oxidation to SOA formation

The concentrations of alkanes, alkenes and aromatics observed at YC were 6.783 ± 3.722, 2.600 ± 1.131 and 1.325 ± 0.749 ppbv, respectively. In terms of anthropogenic species, the concentrations of benzene (0.616 ppbv) and toluene (0.337 ppbv) observed in YC were lower than those in Changdao (benzene = 0.99 ppbv, toluene = 0.59 ppbv), a receptor site in Shandong Province (Yuan et al., 2013). However, the

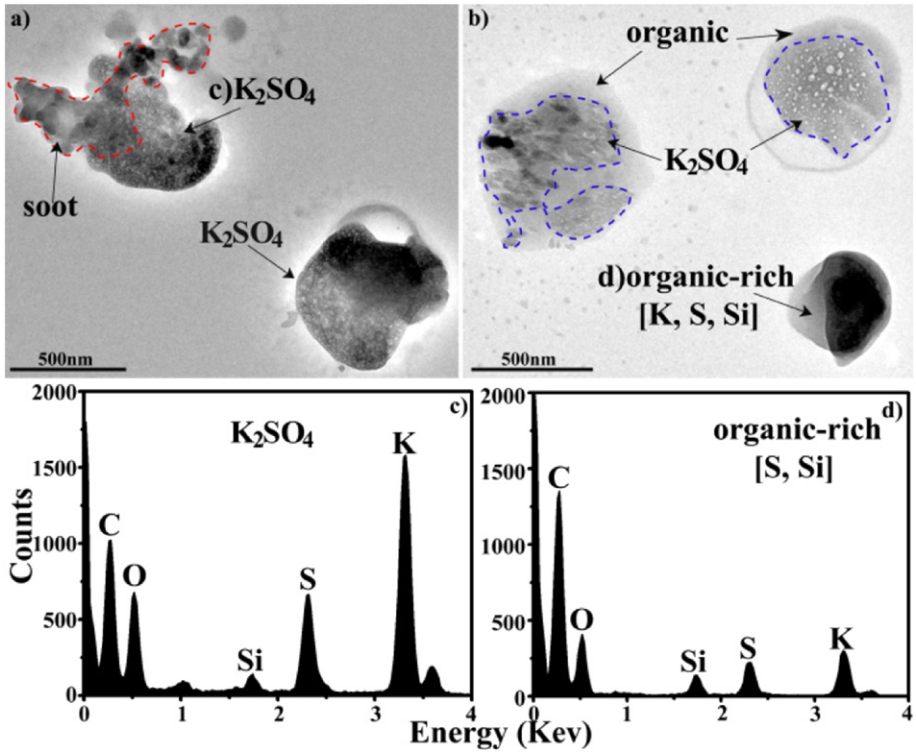

Fig. 8. TEM images and EDX spectra of the mixtures of organic, soot and K-S-rich particles in BB1 (left, 13 June, 08:00) and BB2 (right, 16 June, 08:00).

Table 2
Contribution of biomass burning and the other sources to OC and EC in typical biomass burning events (BB1 and BB2) in summer, 2013. bb: biomass burning and ff: fossil fuel. Data in parenthesis indicate the fraction of OC and EC.

		OC, μgC m^{-3}	EC, μgC m^{-3}
BB1	bb	9.60 (52.6%)	1.91 (51.1%)
	ff	3.65 (20.0%)	1.82 (48.9%)
	SOC	5.01 (27.4%)	–
BB2	bb	9.83 (44.5%)	1.95 (50.8%)
	ff	3.80 (17.2%)	1.89 (49.2%)
	SOC	8.45 (38.3%)	–

isoprene concentration observed at YC (0.375 ± 0.561 ppbv) was much higher than that in Changdao (0.01 ppbv, Yuan et al., 2013). VOC species, especially highly reactive species (e.g. aromatics), are oxidised through photochemical reactions. Some of these products of low vapor pressure condense on the particles to establish equilibrium through gas-particle partitioning and form SOA. Based on the evolution of VOCs, a parameterisation method was proposed to estimate SOA formation from VOC oxidation (SOA_{cal}). A simple description of this method is provided below (Yuan et al., 2013):

$$SOA_{cal} = \sum_i NMHC_{i,consumed} \times Y_i \quad (17)$$

$$NMHC_{i,consumed} = ER_i \times (1 - \exp(-k_{i,OH}[OH]\Delta t)) \quad (18)$$

$$[NMHC_i] = ER_i \times \left([CO] - [CO]_{bg}\right) \times \exp\left[-(k_{i,OH} - k_{CO})[OH]\Delta t\right] \quad (19)$$

$$\Delta t \bullet [OH] = \frac{1}{(k_T - k_B)} \times \left[\ln\left(\frac{[T]}{[B]}|_{t=0}\right) - \ln\left(\frac{[T]}{[B]}\right)\right]. \quad (20)$$

To better understand the evolution of the VOCs, the method is described in reversed order from Eq. (20) to Eq. (17), as follows.

In Eq. (20), T and B denote toluene and benzene, respectively; Δt•[OH] denotes photochemical exposure time; Δt is photochemical age; and [OH] is the average OH-radical concentration (molecules cm^{-3}). k_T and k_B are the OH rate coefficients of toluene (5.63×10^{-12} cm^3 $molecule^{-1}$ s^{-1}) and benzene (1.22×10^{-12} cm^3 $molecule^{-1}$ s^{-1}). $\frac{[T]}{[B]}$ and $\frac{[T]}{[B]}|_{t=0}$ are concentration ratios and the initial emission ratios of toluene and benzene, respectively. $\frac{[T]}{[B]}|_{t=0}$ was calculated using the 97.5 percentile of the T/B ratio, which was 2.88, lower than the equivalent ratio for urban areas (3.7) reported in the New England Air Quality Study (De Gouw et al., 2005). Δt•[OH] was obtained from Eq. (20) and used as a whole in the following calculation. Assuming the average [OH] is 2.6×10^6 molecule cm^{-3}, based on the OH concentration at a rural site in Beijing during summer (Takegawa et al., 2009), then Δt is 16.1 h, using Eq. (20).

In Eq. (19), [$NMHC_i$] and [CO] are the measured concentrations of NMHCs and CO, respectively. $[CO]_{bg}$ is the background concentration, which is determined from the intercept in the scatter plot of CO against benzene (0.097 ppm). $k_{i,OH}$ and k_{CO} are the OH-rate constants for the NMHCs and CO (0.24×10^{-12} cm^3 $molecule^{-1}$ s^{-1}), respectively. ER_i is the emission ratio of NMHCs to CO.·Using an online dataset, Yuan et al. (2013) calculated $k_{i,OH}$ and ER_i by fitting to Eq. (19), and found that the derived $k_{i,OH}$ values compared well with those reported in the literature (Atkinson and Arey, 2003) for species with lower $k_{i,OH}$ values than m + *p*-xylene. In the current study, $k_{i,OH}$ values lower than those of m + p-xylene were obtained from the literature (Atkinson and Arey, 2003) and used to calculate the ERs of *i* species. The ERs for styrene and trimethylbenzene (OH-rate coefficients higher than those of m + p-xylene) were the same as those obtained in Changdao, Shandong by Yuan et al. (2013). The ER and OH-rate coefficient of isoprene were obtained from fits to Eq. (19). This enabled $NMHC_{i,consumed}$, the ratio of consumed NMHC concentration to CO (in $\mu g m^{-3}$ ppm^{-1} CO), to be determined using Eq. (18). Isoprene and C6–C11 NMHC species were used to calculate SOA formation.

In Eq. (17), Y_i denotes the SOA yield of NMHCs obtained from chamber studies. The SOA yield of hydrocarbons has been shown to depend significantly on NOx levels. Ng et al. (2007) investigated SOA formation under low-NOx (<1 ppb) and high-NOx (~1 ppm) conditions, and found that the SOA yield of most aromatics under low-NOx conditions is significantly higher than that under high-NOx conditions. In the current study, the concentrations of NO and NO_2 obtained at YC were 2.3 ± 6.4 ppb and 16.8 ± 11.1 ppb throughout the whole campaign in 2014. Therefore, we calculated the SOA formed from VOC oxidation under low-NOx and high-NOx conditions separately. The results are displayed in Table 3.

The SOA derived from VOC oxidation comprised 3.21 $\mu g m^{-3}$ ppm^{-1} CO under low-NOx conditions and 1.07 $\mu g m^{-3}$ ppm^{-1} CO under high-NOx conditions. Aromatics were the most significant contributor to SOA formation, accounting for 88.4% and 80.6% of the SOA formed from the measured VOCs under low-NOx and high-NOx conditions, respectively. Benzene, toluene, xylene and ethylbenzene were the dominant SOA precursors under both low-NOx and high-NOx conditions (Table 3). SOA formation from isoprene oxidation accounted for 8.6% and 10.3% of SOA_{cal} under low-NOx and high-NOx conditions, respectively. Despite the low SOA yield of isoprene oxidation, isoprene emissions were higher than those of the other VOC species, making isoprene-derived SOA non-negligible. As most of the canister samples were taken during the day, we calculated SOA concentration (SOA = SOC * 2.05; SOC was calculated using the EC-tracer method mentioned in Section 2.2) between 08:00 and 18:00, and obtained a value of 9.80 $\mu g m^{-3}$. Clearly, this result cannot be attributed solely to VOC oxidation. The oxidation of the identified VOCs accounted for only 32.7% and 10.9% of the total SOA concentration under low-NOx and high-NOx conditions, respectively, representing the upper and lower limits of SOA formation from VOC oxidation. There are possible reasons for the large remaining volume of SOA. The first is the presence of unidentified VOCs with a large molecular weight. Semi-volatile organic compounds (SVOCs), which are difficult to detect in the atmosphere, are significant SOA precursors. In a chamber study, SOA yield was found to increase (up to 0.6) as the carbon number of C12-C17 *n*-alkanes increased (Presto et al., 2010). A high SVOC concentration (13.33 μgC m^{-3}) was reported at Mount Tai, an elevated background site in the NCP region (Wang et al., 2011). High concentrations of SVOCs yield large quantities of SOA, generating great SOA production potential. Second, when calculating the concentration of SOA produced from VOC oxidation, we considered only reactions between VOCs and OH radicals during the daytime. As O_3 is an important oxidant in the atmosphere, with a high concentration during the day, reactions between precursor VOCs and O_3 may have contributed to the unexplained proportion of SOA in YC. Aromatics, particularly benzene, toluene, xylene and ethylbenzene and PAHs, should be prioritised in efforts to develop regional measures to control VOCs.

4. Conclusion

The characteristics, biomass burning impact and secondary formation of carbonaceous aerosols in $PM_{2.5}$ were investigated at YC, a rural receptor site on the NCP, during summer 2013 and summer 2014. The carbonaceous aerosols exhibited similar diurnal variation in the two summers, which was associated with meteorological factor. The OM/OC ratio was calculated (2.07 ± 0.05) to provide a new reference for the estimation of organic aerosols in rural areas of the NCP. Frequent biomass burning was observed during the sampling period in 2013, indicating that biomass burning is still an important source of carbonaceous compounds in the NCP region. Morphological particle analysis revealed soot with a collapsed graphitic structure and S- and K-rich particles with organic coatings, indicating that smoke emitted from biomass burning had photochemically aged and that SOA had formed.

Table 3
Emission ratios of VOC species, SOA yields and the SOA formed from VOCs oxidation at YC.

Species	Mixing ratios, μg m^{-3}	ERs, μg m^{-3} ppm^{-1} CO	Yields		SOA formed, μg m^{-3} ppm^{-1} CO		Note
			Low-NOx	High-NOx	Low-NOx	High-NOx	
n-Heptane	0.12	0.32	0.009	0.009	0.002	0.002	(Lim and Ziemann 2009)
n-Octane	0.03	0.07	0.041	0.041	0.002	0.002	(Lim and Ziemann 2009)
n-Nonane	0.06	0.19	0.08	0.08	0.013	0.013	(Lim and Ziemann 2009)
n-Decane	0.07	0.22	0.146	0.146	0.028	0.028	(Lim and Ziemann 2009)
2,4-Dimethylpentane	0.14	0.34	0.009	0.009	0.002	0.002	*n*-Heptane value
2-Methylhexane	0.13	0.33	0.009	0.009	0.002	0.002	*n*-Heptane value
2,3-Dimethylpentane	0.11	0.22	0.009	0.009	0.000	0.000	*n*-Heptane value
3-Methylhexane	0.09	0.22	0.009	0.009	0.001	0.001	*n*-Heptane value
2,2,4-Trimethylpentane	0.06	0.14	0.041	0.041	0.003	0.003	*n*-Octane value
2,3,4-Trimethylpentane	0.02	0.05	0.041	0.041	0.001	0.001	n-Octane value
2-Methylheptane	0.03	0.08	0.041	0.041	0.002	0.002	n-Octane value
3-Methylheptane	0.02	0.05	0.041	0.041	0.001	0.001	n-Octane value
Cyclopentane	0.12	0.29	0.04	0.04	0.007	0.007	Cyclohexane value
Methylcyclopentane	0.18	0.45	0.04	0.04	0.011	0.011	Cyclohexane value
Cyclohexane	0.20	0.54	0.04	0.04	0.015	0.015	(Lim and Ziemann 2009)
Methylcyclohexane	0.04	0.09	0.121	0.121	0.007	0.007	Cycloheptane value
Benzene	2.15	4.39	0.37	0.263	0.315	0.224	(Ng et al. 2007)
Toluene	1.39	3.50	0.30	0.12	0.662	0.265	(Ng et al. 2007)
Ethylbenzene	0.41	1.12	0.36	0.072	0.285	0.057	*m*-Xylene value
m/p-Xylene	0.40	1.91	0.36	0.072	0.664	0.133	(Ng et al. 2007)
o-Xylene	0.19	0.69	0.36	0.072	0.227	0.045	*m*-Xylene value
Styrene	0.13	0.34	0.36	0.072	0.122	0.024	*m*-Xylene value
i-Propylbenzene	0.03	0.09	0.36	0.072	0.021	0.004	m-Xylene value
n-Propylbenzene	0.05	0.12	0.36	0.072	0.027	0.005	*m*-Xylene value
m-Ethyltoluene	0.05	0.19	0.36	0.072	0.059	0.012	*m*-Xylene value
p-Ethyltoluene	0.04	0.19	0.36	0.072	0.064	0.013	*m*-Xylene value
1,3,5-Trimethylbenzene	0.09	0.19	0.36	0.072	0.068	0.014	*m*-Xylene value
o-Ethyltoluene	0.04	0.14	0.36	0.072	0.044	0.009	*m*-Xylene value
1,2,4-Trimethylbenzene	0.18	0.58	0.36	0.072	0.208	0.042	*m*-Xylene value
1,2,3-Trimethylbenzene	0.12	0.19	0.36	0.072	0.068	0.014	*m*-Xylene value
Isoprene	1.139	8.27	0.05[a]	0.02[a]	0.276	0.110	(Kroll et al. 2006)

[a] SOA yields of isoprene under low-NOx and high-NOx condition were averaged from the two lowest NOx and two highest NOx experiments, respectively.

Analysis of the evolution of the VOCs revealed that aromatic species, especially benzene, toluene, xylene and ethylbenzene, were the dominant contributors to SOA formation. Isoprene-derived SOA should be considered in future studies of rural areas of the NCP. The findings of this investigation offer a reference for future attempts to estimate organic-aerosol proportions in rural areas of the NCP, provide intuitive insights into the influence of biomass burning on carbonaceous-aerosol emissions, and indicate the primary species responsible for SOA formation, providing the basis for a regional strategy to control carbonaceous aerosols (or organic aerosols). Nevertheless, more long-term studies are needed to explore the seasonal variation and biomass burning impact on carbonaceous aerosols in other seasons in this area.

Acknowledgements

This work was supported by a Taishan Scholar Grant (TS 20120552), the National Natural Science Foundation of China (Nos 41375126, 41275123, 21190053, 21177025, 21577079 and 21307074), the Fundamental Research Funds of Shandong University (No. 2014GN010), the Shanghai Science and Technology Commission of Shanghai Municipality (Nos 13XD1400700, 12DJ1400100), the Strategic Priority Research Programme of the Chinese Academy of Sciences (No. XDB05010200), Special Research for Public-Beneficial Environment Protection (No. 201009001-1) and the Hong Kong Polytechnic University (No. 4-ZZCQ).

References

Aiken, A.C., Decarlo, P.F., Kroll, J.H., Worsnop, D.R., Huffman, J.A., Docherty, K.S., et al., 2008. O/C and OM/OC ratios of primary, secondary, and ambient organic aerosols with high-resolution time-of-flight aerosol mass spectrometry. Environ. Sci. Technol. 42, 4478–4485.

Atkinson, R., Arey, J., 2003. Atmospheric degradation of volatile organic compounds. Chem. Rev. 103, 4605–4638.

Bae, M.S., Demerjian, K.L., Schwab, J.J., 2006. Seasonal estimation of organic mass to organic carbon in $PM_{2.5}$ at rural and urban locations in New York state. Atmos. Environ. 40, 7467–7479.

Bressi, M., Sciare, J., Ghersi, V., Bonnaire, N., Nicolas, J.B., Petit, J.E., et al., 2013. A one-year comprehensive chemical characterisation of fine aerosol ($PM_{2.5}$) at urban, suburban and rural background sites in the region of Paris (France). Atmos. Chem. Phys. 13, 7825–7844.

Cachier, H., Liousse, C., Buat-Menard, P., Gaudichet, A., 1995. Particulate content of savanna fire emissions. J. Atmos. Chem. 22, 123–148.

Cao, J.J., Lee, S.C., Chow, J.C., Watson, J.G., Ho, K.F., Zhang, R.J., et al., 2007. Spatial and seasonal distributions of carbonaceous aerosols over China. J. Geophys. Res. 112. http://dx.doi.org/10.1029/2006JD008205.

Chen, Y., S.D., Xie, Luo, B., Zhai, C.Z., 2014. Characteristics and origins of carbonaceous aerosol in the Sichuan Basin. China. Atmos. Environ. 94, 215–223.

Chen, Q., Farmer, D.K., Rizzo, L.V., Pauliquevis, T., Kuwata, M., Karl, T.G., et al., 2015. Submicron particle mass concentrations and sources in the Amazonian wet season (AMAZE-08). Atmos. Chem. Phys. 15, 3687–3701.

Cheng, Y., Engling, G., K.B., He, Duan, F.K., Ma, Y.L., Du, Z.Y., et al., 2013. Biomass burning contribution to Beijing aerosol. Atmos. Chem. Phys. 13, 7765–7781.

Cousins, I.T., Beck, A.J., Jones, K.C., 1999. A review of the processes involved in the exchange of semi-volatile organic compounds (SVOC) across the air–soil interface. Sci. Total Environ. 228, 5–24.

De Gouw, J.A., Middlebrook, A.M., Warneke, C., Goldan, P.D., Kuster, W.C., Roberts, J.M., et al., 2005. Budget of organic carbon in a polluted atmosphere: results from the New England air quality study in 2002. J. Geophys. Res. 110. http://dx.doi.org/10.1029/2004JD005623.

Duan, F.K., Liu, X.D., Yu, T., Cachier, H., 2004. Identification and estimate of biomass burning contribution to the urban aerosol organic carbon concentrations in Beijing. Atmos. Environ. 38, 1275–1282.

Fu, H., Zhang, M., Li, W., Chen, J., Wang, L., Quan, X., et al., 2012a. Morphology, composition and mixing state of individual carbonaceous aerosol in urban Shanghai. Atmos. Chem. Phys. 12, 693–707.

Fu, P.Q., Kawamura, K., Chen, J., Li, J., Sun, Y.L., Liu, Y., et al., 2012b. Diurnal variations of organic molecular tracers and stable carbon isotopic composition in atmospheric aerosols over Mt. Tai in the North China Plain: an influence of biomass burning. Atmos. Chem. Phys. 12, 8359–8375.

Gilardoni, S., Vignati, E., Cavalli, F., Putaud, J., Larsen, B., Karl, M., et al., 2011. Better constraints on sources of carbonaceous aerosols using a combined ^{14}C–macro tracer analysis in a European rural background site. Atmos. Chem. Phys. 11, 5685–5700.

Guinot, B., Cachier, H., Oikonomou, K., 2007. Geochemical perspectives from a new aerosol chemical mass closure. Atmos. Chem. Phys. 7, 1657–1670.
Huang, X.F., He, L.Y., Hu, M., Canagaratna, M., Kroll, J., Ng, N., et al., 2011. Characterization of submicron aerosols at a rural site in Pearl River Delta of China using an aerodyne high-resolution aerosol mass spectrometer. Atmos. Chem. Phys. 11, 1865–1877.
Huang, X.F., Xue, L., Tian, X.D., Shao, W.W., Sun, T.L., Gong, Z.H., et al., 2013. Highly time-resolved carbonaceous aerosol characterization in Yangtze River Delta of China: composition, mixing state and secondary formation. Atmos. Environ. 64, 200–207.
Jacobson, M.Z., 2001. Strong radiative heating due to the mixing state of black carbon in atmospheric aerosols. Nature 409, 695–697.
Jung, J.S., Lee, S., Kim, H., Kim, D., Lee, H., Oh, S., 2014. Quantitative determination of the biomass burning contribution to atmospheric carbonaceous aerosols in Daejeon, Korea, during the rice-harvest period. Atmos. Environ. 89, 642–650.
Khalizov, A.F., Lin, Y., Qiu, C., Guo, S., Collins, D., Zhang, R.Y., 2013. Role of OH-initiated oxidation of isoprene in aging of combustion soot. Environ. Sci. Technol. 47, 2254–2263.
Kim, E., Hopke, P.K., 2004. Improving source identification of fine particles in a rural northeastern US area utilizing temperature-resolved carbon fractions. J. Geophys. Res. 109. http://dx.doi.org/10.1029/2003JD004199.
Kondo, Y., Komazaki, Y., Miyazaki, Y., Moteki, N., Takegawa, N., Kodama, D., et al., 2006. Temporal variations of elemental carbon in Tokyo. J. Geophys. Res. 111. http://dx.doi.org/10.1029/2005JD006257.
Kroll, J.H., Ng, N.L., Murphy, S.M., Flagan, R.C., Seinfeld, J.H., 2006. Secondary organic aerosol formation from isoprene photooxidation. Environ. Sci. Technol. 40, 1869–1877.
Lambe, A., Chhabra, P., Onasch, T., Brune, W., Hunter, J., Kroll, J., et al., 2015. Effect of oxidant concentration, exposure time, and seed particles on secondary organic aerosol chemical composition and yield. Atmos. Chem. Phys. 15, 3063–3075.
Lamorena, R.B., Lee, W., 2008. Influence of ozone concentration and temperature on ultrafine particle and gaseous volatile organic compound formations generated during the ozone-initiated reactions with emitted terpenes from a car air freshener. J. Hazard. Mater. 158, 471–477.
Li, W.F., Bai, Z.P., 2009. Characteristics of organic and elemental carbon in atmospheric fine particles in Tianjin, China. Particuology 7, 432–437.
Li, W.J., Shao, L.Y., 2010. Mixing and water-soluble characteristics of particulate organic compounds in individual urban aerosol particles. J. Geophys. Res. 115. http://dx.doi.org/10.1029/2009JD012575.
Li, X.H., Wang, S.X., Duan, L., Hao, J.M., Li, C., Chen, Y.S., et al., 2007. Particulate and trace gas emissions from open burning of wheat straw and corn stover in China. Environ. Sci. Technol. 41, 6052–6058.
Li, W.J., Shao, L.Y., Buseck, P., 2010. Haze types in Beijing and the influence of agricultural biomass burning. Atmos. Chem. Phys. 10, 8119–8130.
Lim, Y.B., Ziemann, P.J., 2009. Effects of molecular structure on aerosol yields from OH radical – initiated reactions of linear, branched, and cyclic alkanes in the presence of NOx. Environ. Sci. Technol. 43, 2328–2334.
Liu, W., Wang, Y., Russell, A., Edgerton, E.S., 2005. Atmospheric aerosol over two urban–rural pairs in the southeastern United States: chemical composition and possible sources. Atmos. Environ. 39, 4453–4470.
Mauderly, J.L., Chow, J.C., 2008. Health effects of organic aerosols. Inhal. Toxicol. 20, 257–288.
Ng, N.L., Kroll, J.H., Chan, A.W.H., Chhabra, P.S., Flagan, R.C., Seinfeld, J.H., 2007. Secondary organic aerosol formation from *m*-xylene, toluene, and benzene. Atmos. Chem. Phys. 7, 3909–3922.
Pathak, R.K., Wang, T., Ho, K.F., Lee, S.C., 2011. Characteristics of summertime $PM_{2.5}$ organic and elemental carbon in four major Chinese cities: implications of high acidity for water-soluble organic carbon (WSOC). Atmos. Environ. 45, 318–325.
Presto, A.A., Miracolo, M.A., Donahue, N.M., Robinson, A.L., 2010. Secondary organic aerosol formation from high-NOx photo-oxidation of low volatility precursors: *n*-alkanes. Environ. Sci. Technol. 44, 2029–2034.
Ramanathan, V., Carmichael, G., 2008. Global and regional climate changes due to black carbon. Nature Geosci. 1, 221–227.
Rollins, A., Browne, E., Min, K.E., Pusede, S., Wooldridge, P., Gentner, D., et al., 2012. Evidence for NOx control over nighttime SOA formation. Science 337, 1210–1212.
Russell, L.M., 2003. Aerosol organic-mass-to-organic-carbon ratio measurements. Environ. Sci. Technol. 37, 2982–2987.
Sahu, L., Kondo, Y., Miyazaki, Y., Pongkiatkul, P., Kim, O.N., 2011. Seasonal and diurnal variations of black carbon and organic carbon aerosols in Bangkok. J. Geophys. Res. 116. http://dx.doi.org/10.1029/2010JD015563.
Seinfeld, J.H., Pandis, S.N., 1998. Atmospheric Chemistry and Physics: From Air Pollution to Climate Change 1360 pp. John Wiley, Hoboken, NJ.
Szidat, S., Jenk, T.M., Synal, H.A., Kalberer, M., Wacker, L., Hajdas, I., et al., 2006. Contributions of fossil fuel, biomass-burning, and biogenic emissions to carbonaceous aerosols in Zurich as traced by ^{14}C. J. Geophys. Res. 111. http://dx.doi.org/10.1029/2005JD006590.
Takegawa, N., Miyakawa, T., Kuwata, M., Kondo, Y., Zhao, Y., Han, S., et al., 2009. Variability of submicron aerosol observed at a rural site in Beijing in the summer of 2006. J. Geophys. Res. 114. http://dx.doi.org/10.1029/2008JD010857.
Turpin, B.J., Lim, H.J., 2001. Species contributions to $PM_{2.5}$ mass concentrations: revisiting common assumptions for estimating organic mass. Aerosol Sci. Technol. 35, 602–610.
Wang, B., Shao, M., Lu, S.H., Yuan, B., Zhao, Y., Wang, M., et al., 2010. Variation of ambient non-methane hydrocarbons in Beijing city in summer 2008. Atmos. Chem. Phys. 10, 5911–5923.
Wang, Z., Wang, T., Gao, R., Xue, L.K., Guo, J., Zhou, Y., et al., 2011. Source and variation of carbonaceous aerosols at Mount Tai, North China: results from a semi-continuous instrument. Atmos. Environ. 45, 1655–1667.
Wang, Z., Wang, T., Guo, J., Gao, R., Xue, L.K., Zhang, J.M., et al., 2012. Formation of secondary organic carbon and cloud impact on carbonaceous aerosols at Mount Tai, North China. Atmos. Environ. 46, 516–527.
Wen, L., Chen, J.M., Yang, L.X., Wang, X.F., Xu, C.H., Sui, X., et al., 2015. Enhanced formation of fine particulate nitrate at a rural site on the North China Plain in summer: the important roles of ammonia and ozone. Atmos. Environ. 101, 294–302.
Xing, L., Fu, T.M., Cao, J.J., Lee, S.C., Wang, G.H., Ho, K.F., et al., 2013. Seasonal and spatial variability of the OM/OC mass ratios and high regional correlation between oxalic acid and zinc in Chinese urban organic aerosols. Atmos. Chem. Phys. 13, 4307–4318.
Xue, L.K., Wan, T., Zhang, J.M., Zhang, X.C., Deliger, Poon, C.N., et al., 2011. Source of surface ozone and reactive nitrogen speciation at Mount Waliguan in western China: new insights from the 2006 summer study. J. Geophys. Res. 116, doi: http://dx.doi.org/10.1029/2010JD014735.
Yan, M.C., Gu, T.X., Chi, Q.H., Wang, C.S., 1997. Abundance of chemical elements of soils in China and supergenesis geochemistry characteristics. Geophys. Geochem. Explor. 21, 161–167 (in Chinese).
Yang, F., Huang, L., Duan, F., Zhang, W., He, K., Ma, Y., et al., 2011. Carbonaceous species in $PM_{2.5}$ at a pair of rural/urban sites in Beijing, 2005–2008. Atmos. Chem. Phys. 11, 7893–7903.
Yang, L.X., Zhou, X.H., Wang, Z., Zhou, Y., Cheng, S.H., Xu, P.J., et al., 2012. Airborne fine particulate pollution in Jinan, China: concentrations, chemical compositions and influence on visibility impairment. Atmos. Environ. 55, 506–514.
Yuan, B., Hu, W.W., Shao, M., Wang, M., Chen, W.T., Lu, S.H., et al., 2013. VOC emissions, evolutions and contributions to SOA formation at a receptor site in eastern China. Atmos. Chem. Phys. 13, 8815–8832.
Zhang, R.Y., Khalizov, A.F., Pagels, J., Zhang, D., Xue, H.X., McMurry, P.H., 2008a. Variability in morphology, hygroscopicity, and optical properties of soot aerosols during atmospheric processing. Proc. Natl. Acad. Sci. U. S. A. 105, 10291–10296.
Zhang, T., Claeys, M., Cachier, H., Dong, S.P., Wang, W., Maenhaut, W., et al., 2008b. Identification and estimation of the biomass burning contribution to Beijing aerosol using levoglucosan as a molecular marker. Atmos. Environ. 42, 7013–7021.
Zhang, Q., Streets, D.G., Carmichael, G.R., He, K., Huo, H., Kannari, A., et al., 2009. Asian emissions in 2006 for the NASA INTEX-B mission. Atmos. Chem. Phys. 9, 5131–5153.
Zhao, P.S., Dong, F., Yang, Y.D., He, D., Zhao, X.J., Zhang, W.Z., et al., 2013. Characteristics of carbonaceous aerosol in the region of Beijing, Tianjin, and Hebei. China. Atmos. Environ. 71, 389–398.
Zhou, S.Z., Wang, Z., Gao, R., Xue, L.K., Yuan, C., Wang, T., et al., 2012. Formation of secondary organic carbon and long-range transport of carbonaceous aerosols at Mount Heng in South China. Atmos. Environ. 63, 203–212.
Zhu, Y.H., Yang, L.X., Chen, J.M., Wang, X.F., Xue, L.K., Sui, X., et al., 2015. Characteristics of ambient volatile organic compounds and the influence of biomass burning at a rural site in Northern China during summer 2013. Atmos. Environ. http://dx.doi.org/10.1016/j.atmosenv.2015.08.097.